Journal of Applied Polymer Science

# Fracture Mechanical Analysis of Two Commercial Polyoxymethylene Homopolymer Resins

**Michael Berer,[1] Gerald Pinter,[2] Michael Feuchter[1,2]**
[1]Polymer Competence Center Leoben GmbH, Leoben 8700, Austria
[2]Materials Science and Testing of Polymers, Montanuniversitaet Leoben, Leoben 8700, Austria
Correspondence to: M. Berer (E-mail: michael.berer@pccl.at)

**ABSTRACT:** This research addresses the fracture mechanical analysis of two commercially available polyoxymethylene homopolymer resins. Two types of experiments are used: monotonic fracture toughness tests and cyclic fatigue crack growth tests. The resulting total lifetimes in the fatigue crack growth tests are split up into the appropriate parts of crack growth initiation and fatigue crack propagation. Fracture surfaces of monotonic and cyclic tests are analyzed using light microscopy and scanning electron microscopy. Besides the mechanical tests, the morphology within the used compact tension specimens is examined in detail by using differential scanning calorimetry, small- and wide-angle X-ray scattering, and polarized light microscopy. The results are analyzed and discussed, considering observations in the previous studies published in the literature. It is shown that both materials can be well analyzed using linear elastic fracture mechanics and their fracture mechanical properties are presented in conjunction with a detailed documentation of the microstructure. © 2014 Wiley Periodicals, Inc. J. Appl. Polym. Sci. **2014**, *131*, 40831.

**KEYWORDS:** mechanical properties; microscopy; morphology; structure-property relations; thermoplastics

Received 20 November 2013; accepted 6 April 2014
**DOI: 10.1002/app.40831**

## INTRODUCTION

Polyoxymethylene (POM) is a semicrystalline thermoplastic which is widely used in practical applications.[1,2] Owing to its good friction and wear behavior, it is used in tribological and contact applications such as gear wheels[3,4] or bearing elements which were recently investigated by the author.[5,6] In the latter case, not only tribological properties are important but also time-dependent mechanical behavior and fatigue resistance of the materials are crucial. The time dependence of POM and its effects on the rolling performance of bearing elements were analyzed in the previously published studies.[5,6] In contrast, the information regarding fatigue of the bearing elements has been based on the literature so far.[7–11]

Therefore, the goal of this study was to analyze the fatigue resistance of two commercially available POM homopolymer resins using the fracture mechanics approach. For this purpose, monotonic fracture tests and cyclic fatigue crack growth tests were carried out. For the data analysis, the linear elastic fracture mechanics (LEFM) concept was used, whose general applicability for polymers is documented in the literature.[12–14] The generated fracture surfaces were analyzed and discussed using the information available in the literature. Besides the fracture mechanical analysis, the fatigue test data were also examined concerning the dynamic mechanical behavior of the specimen during the test. To elaborate the differences between the materials, a basic material characterization in combination with a detailed analysis of the morphology within the specimens was conducted.

## EXPERIMENTAL

### Materials and Specimens

Two different POM homopolymer types were used in this study. The first POM type ("Tenac 3010") was provided by Asahi Kasei (Asahi Kasei, Tokyo, Japan) and the second one ("Delrin 100") by DuPont (DuPont, Wilmington, DE). Both materials were selected because they are commercially available standard materials of very similar properties. Additionally, Delrin 100 has been used for many years and thus information is available for this material in the literature. This facilitates the interpretation of the results and the comparison with Tenac 3010. The materials will be denoted as "Tenac" and "Delrin" in this research.

All tensile tests were conducted with injection-molded multipurpose specimens according to ISO 3167 (Type A). Fracture mechanical examinations were made with injection-molded compact tension (CT) specimens which were produced in accordance with international standards (e.g., ISO 13586 and ISO 15850). The "effective width" ($w$) of these CT specimens was 40 mm and their thickness ($h$) was 4 mm. The specimens

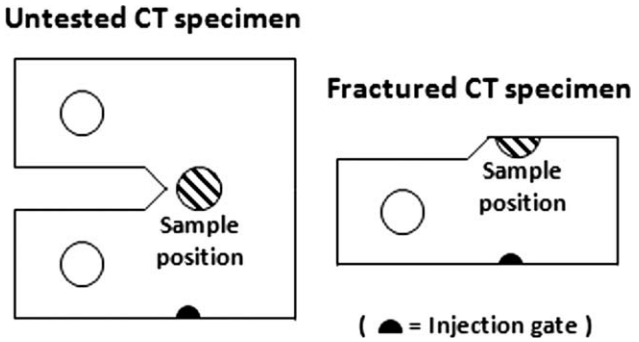


**Figure 1.** CT specimens: location of the injection gate and selected position for the basic material characterization.

of both materials were produced with similar processing parameters: identical melt temperature (215°C), identical mold temperature of 90°C, similar injection speed (35 mm $s^{-1}$), and holding pressure (800 bar, 8 s). After releasing the holding pressure, the specimens were further cooled in the mold for another 8 s. The position of the injection gate is shown in Figure 1. The materials were processed without previous or subsequent drying steps.

## METHODS

### Basic Material Characterization

In this section, the methods used for the examination of the basic material characteristics are described. This investigation was conducted to document the state of the materials used for the subsequent fracture mechanical analysis.

**Tensile Tests.** The tensile tests were performed with a tensile testing machine of the type "Zwick Z010" (Zwick/Roell GmbH & Co. KG, Ulm, Germany). An extensometer of the type "BTX-EX-MAKRO.001" (Zwick/Roell GmbH & Co. KG, Ulm, Germany) with a gauge length of 50 mm was used for the strain measurement of up to 25% of strain. Afterwards, the extensometer was removed automatically and strains were calculated using crosshead displacement and clamping length (115 mm). The tensile properties were investigated at three different testing rates (deformation rates: 0.1, 1, and 10 mm $s^{-1}$; strain rates: 8.7 $\times$ $10^{-4}$ $s^{-1}$, 8.7 $\times$ $10^{-3}$ $s^{-1}$, and 8.7 $\times$ $10^{-2}$ $s^{-1}$) for both materials. The tests were conducted at 23°C and 50% of humidity.

**Degree of Crystallinity.** The degree of crystallinity was determined by differential scanning calorimetry (DSC). It was examined for CT specimens of both POM types (Tenac 3010 and Delrin 100). To check for possible changes in the degree of crystallinity owing to the crack growth process, measurements were carried out not only on untested but also on fatigued specimens. The sample position within the CT specimens is shown in Figure 1. It represents the location where the crack growth process occurs during the fatigue tests. It should be noted that the untested specimens had to be broken in advance to get the appropriate material samples. This was done with a chisel and a hammer at the bottom of the machined specimen notch. No cutting process was used to avoid the changes of the material owing to frictional heating. Concerning the fatigued specimen, the samples were taken as close to the fracture surface as possible.

From the samples generated from the CT specimens, 5–7 mg parts were cut out and used for the DSC analysis. The samples were heated at 10 K $min^{-1}$ up to 230°C and the specific heat of fusion was determined. For the calculation of the degree of crystallinity, the specific heat of fusion was divided by the specific heat of fusion of 100% crystalline POM which is 250 J $g^{-1}$ in the case of a homopolymer (according to Plummer et al.[15]). For both materials, two untested and one fatigued CT specimen were analyzed and in each case three repeated measurements were taken. All experiments were conducted on the DSC device "Mettler Toledo DSC 821e" (Mettler Toledo AG, Schwerzenbach, CH) using standard pans.

In addition to the DSC measurements, the degree of crystallinity of one untested CT specimen of Delrin was determined using wide-angle X-ray diffraction (WAXD). For this the device, "NanoStar" (Bruker AXS, Karlsruhe, Germany) was used. To enable comparability, the measurement position was the same as used for the DSC analysis shown in Figure 1. The crystallinity was calculated using eq. (1) in which $I_C$ is the sum of the scattered intensities of crystalline peaks and $I_T$ is the total scattering intensity.[16]

$$\alpha_{WAXD} = \frac{I_C}{I_T} \times 100\% \quad (1)$$

**Spherullite Size and Distribution.** The spherullite size and distribution inside of untested CT specimens was qualitatively investigated by generating thin microtome cuts and analyzing them using polarized light in a light microscope (microscope type: "Olympus BX51", Olympus, Vienna, Austria). Both POM types were examined. Similar to the DSC measurements, the microtome cuts were taken from the sample positions as shown in Figure 1 to ensure comparability between both examinations. The untested specimens were broken as described above for the DSC measurements. The cuts were created with the microtome device "Microtome Reichert Jung" (Reichert Jung, Heidelberg, Germany) with a thickness of approximately 10 μm.

**Long Period and Lamellar Thickness.** For both materials, long period and lamellar thickness of an untested CT specimen were determined using small-angle X-ray scattering (SAXS). The device used for these measurements was the same as used for the WAXD analysis ("NanoStar," Bruker AXS, Karlsruhe, Germany) but with increased distance between sample and detector. Moreover, the measurement position on the CT specimens was approximately the same as used for the WAXD and DSC experiments (Figure 1). To determine the long period of the polymer, the scattering curves were corrected for background scatter. SAXS analyses were performed for the determination of the crystalline thickness and the amorphous interlayer spacing by applying a correlation function method.[17]

**Molecular Weight.** The molecular weight of both materials was analyzed using gel permeation chromatography. Combining this technique with a light scattering detector, the absolute value of the weight-average molecular weight was obtained. In a second step, the system was conventionally calibrated using internal

standards based on narrowly distributed polymethylmethacrylate and a polydispersity index related to these standards was determined. The samples were taken from the sample position shown in Figure 1.

### Fracture Mechanical Analysis

All fracture mechanical investigations were conducted on servo-hydraulic testing machines of the type "MTS 858.02 horizontal" and "MTS 858.14 AT" (MTS, Eden Prairie, MN). For the determination of the crack-opening displacement, the piston displacement was used instead of an extensometer because its accuracy was sufficient for the tests according to our experience. The actual crack length of the specimens was detected optically with a traveling microscope which had a lens magnification of 20 (lens: Marcel Aubert SA, Bienne, Switzerland; adjustable desk: Mitutoyo, Tokyo, Japan). All CT specimens examined were prenotched with a thin razor blade to guarantee uniform crack geometries. The prenotches were 1–2 mm in depth.

Selected fracture surfaces were analyzed using light microscopy and scanning electron microscopy (SEM). The following devices were used for this examination: light microscope "Olympus SZX12" (Olympus, Vienna, Austria) and scanning electron microscope "DSM 962" (Carl Zeiss, Oberkochen, Germany).

**Critical Stress Intensity Factor—$K_C$.** CT specimens of both POM types (Tenac and Delrin) were monotonically torn apart with 10 and 100 mm $min^{-1}$, respectively. In each case, the measurements were repeated at least two times. These two piston deformation rates were chosen because of experience with other polymeric materials. Before starting the test, the initial crack length was determined with the mounted traveling microscope. Both force and displacement were recorded during the test and the appropriate force–displacement curve was generated. From the force–displacement curve, the maximum force was used to calculate the critical stress intensity factor. Owing to the rather small thickness of the CT specimens (4 mm), the critical stress intensity factor values obtained are not expected to be pure plane strain results and thus they are denoted as "$K_C$" instead of "$K_{IC}$."

**Fatigue Crack Growth Tests.** In the fatigue crack growth tests, the specimens were loaded with a sinusoidal signal of 10 Hz frequency and a load ratio, $R$ ($F_{min}/F_{max}$), of 0.1 was used for all tests. Furthermore, the experiments were made in load-controlled mode with varying initial stress intensity factor ranges ($\Delta K_{init}$). During the tests, peak/valley pairs of force and displacement were recorded every 100 cycles together with the corresponding cycle number. Additionally, complete hysteresis curves (force, displacement, and time) were recorded every 1000 cycles. The peak/valley pairs of force and displacement were transformed into the dynamic specimen compliance ($C_{Dyn}$) according to eq. (2). $C_{Dyn}$ was the basis for further analysis of the recorded results. In addition, the tests were stopped periodically to measure the actual crack length ($a$) with the mounted traveling microscope. Every time the test was stopped, an additional peak/valley pair of force and displacement was recorded (together with the cycle number) and thus actual crack length and actual mechanical behavior ($C_{Dyn}$) could be correlated.

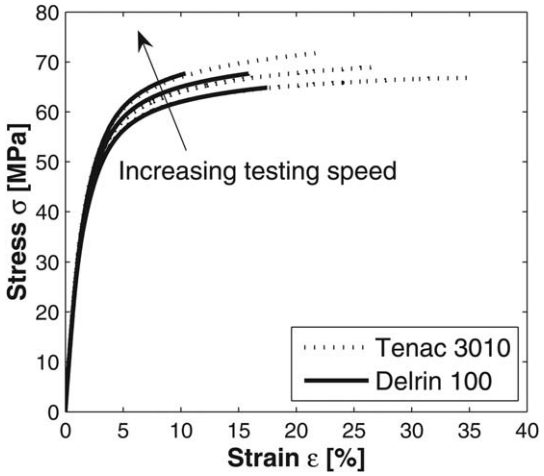


**Figure 2.** Technical stress–strain curves of Tenac and Delrin for different testing rates (deformation rates: 0.1, 1, and 10 mm $s^{-1}$; strain rates: 8.7 × 10-(4 s-(1, 8.7* (10-(3 s-(1, and 8.7* (10-(2 s-(1).

$$C_{Dyn} = |C^*| = \frac{d_{max} - d_{min}}{F_{max} - F_{min}} \quad (2)$$

$C_{Dyn}$ is the dynamic specimen compliance which is equivalent to $|C^*|$ the absolute value of the complex dynamic specimen compliance. $d_{max}$ and $d_{min}$ are the peak/valley data of the displacement; $F_{max}$ and $F_{min}$ are the corresponding peak/valley data of the force.

From the recorded results, crack growth curves and finally crack growth kinetics curves were developed. The detailed method for this procedure was presented and discussed by Berer and Pinter[18] and thus only a short summary will be given here. First, the optically measured crack lengths and their correlated dynamic specimen compliance values were used to create a calibration fit in the form $a = function(C_{Dyn})$. This calibration fit was used to transform the continuously measured dynamic specimen compliance (peak/valley pairs of force and displacement every 100 cycles) into appropriate crack lengths and thus into crack growth curves (transformation of $C_{Dyn}$ = *function* [cycle number] into $a = function$[cycle number]). The crack growth curves were finally used to develop crack growth kinetic curves. Therefore, local polynomials were fit along the crack growth curve and the crack growth rate ($da/dN$) as well as the range of the stress intensity factor ($\Delta K$) was calculated. A more detailed explanation of the method is described in the corresponding literature.[18]

## RESULTS AND DISCUSSION

### Basic Material Characterization

Basic morphological characteristics are presented and compared for both materials in the following section. The morphological investigation is intended as documentation of the materials' state within the specimens. In addition, it allows conclusions concerning the observed fracture mechanical behavior.

### Tensile Tests

Exemplary (technical) stress–strain curves of both materials investigated in this research are shown in Figure 2. Although there is some expected influence of the testing rate, the shape of

**Table I.** DSC- and WAXD-determined Degrees of Crystallinity of Untested and Fatigued CT Specimens (for the Measurement Position, see Figure 1)

| Material | CT specimen | Degree of crystallinity (%) | Number of measurements |
|---|---|---|---|
| Tenac (DSC) | # 1 (Untested) | 65 | 3 |
| | # 2 (Untested) | 65 | 3 |
| | # 3 (Fatigued) | 64 | 3 |
| Delrin (DSC) | # 1 (Untested) | 66 | 3 |
| | # 2 (Untested) | 65 | 3 |
| | # 3 (Fatigued) | 65 | 3 |
| Delrin (WAXD) | # 1 (Untested) | 61 | Single measurement |

the curves is almost identical for both materials. Interestingly, the only significant difference can be found for the strain at break which is higher for Tenac than for Delrin (approximately a factor of 2).

### Degree of Crystallinity

DSC determined degrees of crystallinity of untested and fatigued CT specimens are listed in Table I. Apparently, both POM materials had identical degrees of crystallinity in their initial state and no significant change in this parameter was induced by the crack growth process.

The degree of crystallinity in Table I which was determined by WAXD has a slightly lower level. However, it is in good agreement with what was expected for the following reasons. Although the specimen surface layer which is expected to be less crystalline was removed during the DSC sample preparation, the whole specimen thickness was examined by WAXD. In addition, it was shown by Ostberg and Seferis[19] that the heating process during the DSC measurement is often accompanied by recrystallization of the material. According to that study, the intensity of this recrystallization process strongly depends on the initial state of the material (i.e., deviation from the equilibrium state). Taking into account the degrees of crystallinity of POM reported in the literature (copolymer[8,9,11] and homopolymer[15]) and considering the comparatively high molecular weight of the material types examined, the determined level of crystallinity is a typical one. Thus, it is expected that the material is close enough to its equilibrium state to cause only slight increases in the crystallinity during DSC runs. These two aspects (WAXD value includes specimen surface layer, slight recrystallization during DSC runs) should be considered when comparing the degrees of crystallinity determined by DSC and WAXD.

### Spherullite Size Distribution

It has to be emphasized at this point that the spherullite size distribution was examined to qualitatively indicate morphological differences within and between the specimens. It is not expected to have a direct influence on the fracture mechanical behavior of the investigated POM materials.[8,11,20] In Figure 3, exemplary images of the spherullite size distribution of Tenac and Delrin are shown. Contrary to our previous experience with polyethylene, the spherullite borders of these two POM materials are not distinct. Thus, the image looks confusing at first view. Nevertheless, single spherullites can be identified (markings, Figure 3).

The analysis of the created microtome cuts in direction of the specimen thickness indicated differences in the spherullite size distribution between Tenac and Delrin. Underneath a more or less transparent specimen surface layer, Tenac revealed comparatively large spherullites, whereas the microstructure of Delrin in this area was much finer. Toward the center of the specimen, the microstructure of both materials changed. It became finer for Tenac and coarser for Delrin. Hence, in the middle of the specimen, the microstructure of Tenac was finer compared to Delrin. These observations are interesting as they show slight differences in the morphology of Tenac and Delrin which are not reflected by the degree of crystallinity. Generally, the spherullite size trend observed in Delrin represents what is expected for injection-molded specimens, whereas the trend in Tenac is rather surprising.

The spherullite diameters shown in Figure 3 are in the order of 10–40 μm depending on the exact measurement position. A

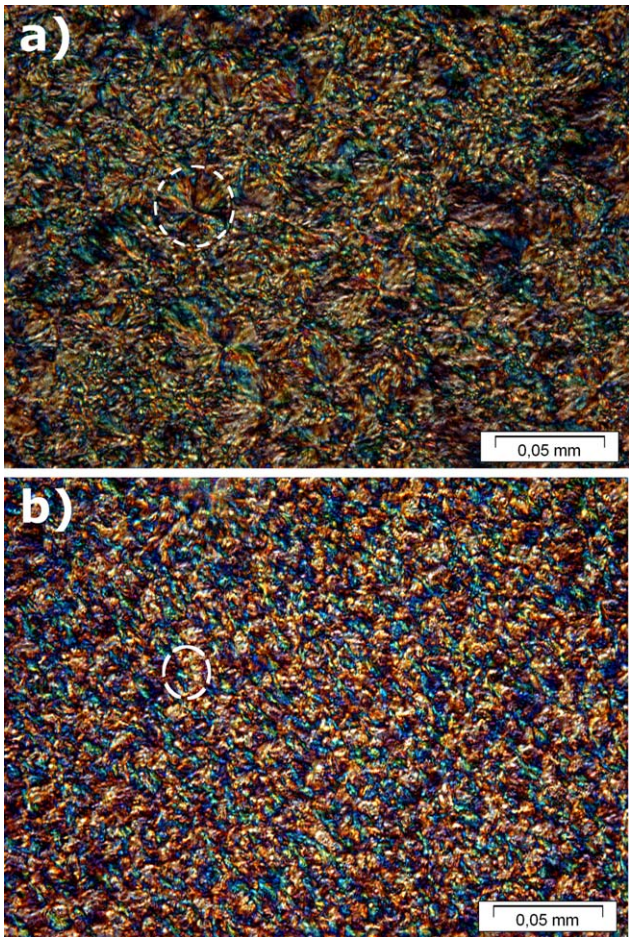


**Figure 3.** Examples of microtome cuts of (a) Tenac and (b) Delrin analyzed using polarized light microscopy and presented in more magnified scale (white markings indicate representative spherullites). [Color figure can be viewed in the online issue, which is available at wileyonlinelibrary.com.]

**Table II.** Results of SAXS Examinations of Untested CT Specimens (Single Measurements)

| Material | Long period (nm) | Thickness of amorphous layer (nm) | Lamellar thickness (nm) | Degree of crystallinity (vol %) |
|---|---|---|---|---|
| Tenac | 13.6 | 3.6 | 10.0 | 74 |
| Delrin | 14.7 | 3.7 | 11.0 | 75 |

spherullite size of approximately 20 μm on fracture surfaces of POM copolymers was reported by Lazzeri et al.[11] In the study by Runt and Gallagher,[8] spherullite diameters of a POM copolymer in dependence on thermal history and nucleation were investigated. In this study, diameters of approximately 35–175 μm in the case of no nucleation and approximately 20 μm for nucleated materials were found for the different heat treatments. Although differences in the crystallization behavior of POM copolymers and POM homopolymers are expected, the comparatively small diameters found in Figure 3 indicate that both of the examined materials (Tenac and Delrin) might be (differently) nucleated. The rather unexpected spherullite size distribution in the abovementioned Tenac CT specimen is also assumed to be a nucleation effect.

### Long Period and Lamellar Thickness

Microstructural parameters, which were determined using SAXS, are listed in Table II. Interestingly, there are small structural differences between Tenac and Delrin (long period) but the volumetric degree of crystallinity (lamellar thickness/long period) is nearly identical. This is similar to the results obtained by the DSC measurements which also gave almost identical degrees of crystallinity for both materials. The level of the volumetric degrees of crystallinity obtained by the SAXS examinations is much higher than the corresponding results of the measurements of DSC and WAXD. This aspect is attributed to error influences on SAXS experiments described in Ref. 21. Similar lamellar thicknesses to those presented in Table II were also found for POM copolymers (approximately, 10–25 nm).[8]

### Molecular Weight

As summarized in Table III, for both materials very similar weight-average molecular weights and polydispersity indices were found experimentally. This means that length and length distribution of the molecules are almost identical for both investigated materials. Comparing the results with values of Delrin 100 reported in the literature (Table III), both materials show good agreement of the weight-average molecular weight. However, the polydispersity index is slightly higher than reported by Bretz et al.[7]

**Table III.** Experimentally Determined Values of Important Molecular Weight Parameters

| Material | Weight-average molecular weight ($M_W$) (g mol$^{-1}$) | Polydispersity index |
|---|---|---|
| Tenac | 137,000 | 2.6 |
| Delrin | 146,000 | 2.6 |
| Delrin (literature[7]) | 140,000 | 2 |

**Table IV.** Critical Stress Intensity Factors ($K_C$) of Tenac and Delrin Determined at Two Different Loading Rates

| | 10 mm min$^{-1}$ | | 100 mm min$^{-1}$ | |
|---|---|---|---|---|
| Material | $K_C$ (MPa m$^{0.5}$) | Standard deviation (MPa m$^{0.5}$) | $K_C$ (MPa m$^{0.5}$) | Standard deviation (MPa m$^{0.5}$) |
| Tenac | 6.7 | 0.15 | 5.5 | 0.47 |
| Delrin | 6.2 | 0.35 | 5.8 | 0.40 |

Assuming the entanglement density to be the critical morphological parameter concerning crack growth resistance and considering the similar molecular weights, differences in the fracture mechanical behavior of both materials can be explained only by varying material morphology. As the specimens of both materials were produced with similar processing parameters, these differences in the fracture mechanical behavior and thus in the material morphology are more general characteristics of the examined POM resins.

### Fracture Mechanical Analysis

**Critical Stress Intensity Factor—$K_C$.** The determined critical stress intensity factors of Tenac and Delrin are summarized in Table IV. Compared to the results reported in the literature (homopolymer[7,20,22] and copolymer[11]), the values listed in Table IV are higher. This is attributed to the comparatively high molecular weight of the materials used in our study and the rather small thickness of the CT specimens (4 mm). At the slower testing rate (10 mm min$^{-1}$), $K_C$ of Tenac is slightly higher than that of Delrin. However, there is no significant difference between the materials at 100 mm min$^{-1}$. Interestingly, $K_C$ of Tenac (Table IV) shows a distinct dependence on the testing rate, whereas in the case of Delrin this testing rate dependence is small and the difference in $K_C$ is almost within the scatter range.

Light microscope images of typical fracture surfaces of monotonically loaded CT specimens are shown in Figure 4. Tenac CT specimens are shown in Figure 4 for illustration purposes though fracture surfaces of Delrin look very similar. Three different areas (marked with 1–3) can be identified in Figure 4(a,b). The first one (in crack growth direction) represents the prenotch which was generated with the razor blade. The second and third areas show the fracture surface generated by crack growth. Especially interesting is the second area with its intensive white color. Similar white zones were found for three-point bent single-edge-notched (SEN) specimens of POM, polyvinyl chloride, and polypropylene.[12] According to the descriptions described by Hertzberg and Manson,[23] where these kinds of zones are also mentioned, this area is interpreted as plastic zone. Contrary to suggestions there, the white color is attributed to microvoids within the material which were generated during the formation of crazes.[15,20,24] As expected, the size of the plastic zone is strongly influenced by the deformation rate

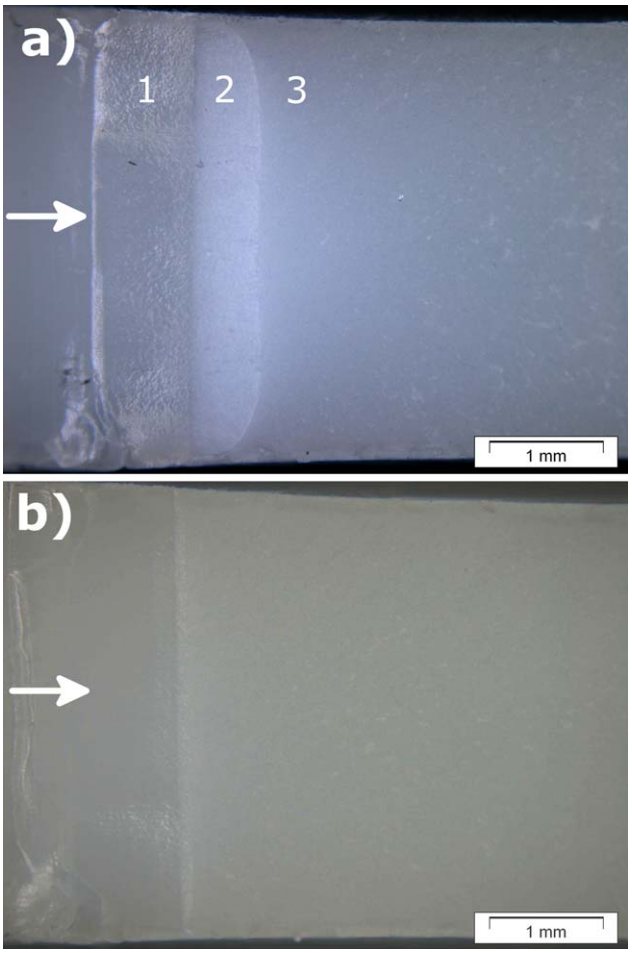


**Figure 4.** Fracture surfaces of Tenac CT specimens loaded monotonically with a deformation rate of (a) 10 mm $min^{-1}$ and (b) 100 mm $min^{-1}$—annotations: (1) razor blade prenotch, (2) craze zone, and (3) spontaneous crack growth (arrow indicates crack growth direction). [Color figure can be viewed in the online issue, which is available at wileyonlinelibrary.com.]

[Figure 4(a,b)]. Thus, in Table V, plastic zone dimensions are presented for the Tenac specimens shown in Figure 4 and for two selected Delrin specimens. Additionally, the measured values are compared to the values calculated using eq. (3) which estimates the plastic zone radius under plane strain conditions.[23] Despite the rather small thickness of the tested CT specimens, the measured plastic zone sizes are smaller than expected for plane strain conditions, which is indeed surprising. The third area in Figure 4 does not show a significant change in color but it appears more matt than the prenotch. This area is related to the spontaneous crack growth which occurred after the crack growth initiation (CGI). According to Hertzberg and Manson,[23] it is generally observed that there is no change in color in this zone.

$$r_p = \frac{1}{6\Pi}\left(\frac{K_c}{\sigma_y}\right)^2 \quad (3)$$

With $r_p$ being the radius of the plastic zone; $K_C$ is the critical stress intensity factor; $\sigma_y$ is the yield stress which was assumed to be 60 MPa for both materials according to Figure 2.

The plastic zones, which were found on the fracture surfaces in Figure 4, are reflected by slight nonlinearity in force–displacement curves recorded during the monotonic loading of CT specimens. However, once the spontaneous crack growth was initiated the specimens broke in a brittle manner without further plastic deformation. Additionally, it should be noted that during the spontaneous crack growth, the crack did not bifurcate but remained within its original plane (perpendicular to the direction of loading).

To extend the understanding of the crack growth mechanism in monotonically loaded specimens of Tenac and Delrin, SEM images of fracture surfaces were generated. The results are shown in Figure 5 for Tenac (same specimen as shown in Figures 4(a)) and in Figure 6 for Delrin. In both the figures, the border between the plastic zone and the spontaneous crack growth zone is represented. The differences in the surface structure of these two zones are clearly visible in both the figures. In the plastic zones, the surface looks rather doughy with smooth structures oriented in the direction of the crack growth. In some cases, these structures have the appearance of material drawn and torn apart. The fracture surface of the spontaneous crack growth shows a completely different texture and is more like a craggy and rocky landscape. Both observations agree well with what was reported for fracture surface structures of tensile-tested POM homopolymer specimens (unnotched tensile specimens and SEN specimens).[22,24] No morphological characteristics (like spherullite structures) are visible on the fracture surfaces as shown in Figures 5 and 6, which is in accordance with the previously published observations.[24]

Comparing Figures 5 and 6, the fracture surfaces of both POM types are very similar at the first view. However, analyzing them in more detail shows that there are interesting differences between the materials. One difference concerns the texture of the plastic zone which is more distinct in Figure 5(a) (Tenac) than in Figure 6(a) (Delrin). Even more interesting is the

**Table V.** Measured and Calculated (using eq. 3) Dimension of the Plastic Zone ($d_p$), Value in Parenthesis Represents the Corresponding Measured $K_C$ Value in MPa $m^{0.5}$

| | 10 mm $min^{-1}$ | | 100 mm $min^{-1}$ | |
|---|---|---|---|---|
| Material | $d_p$ Measured (mm) | $d_p$ Calculated ($d_p = 2r_p$) (mm) | $d_p$ Measured (mm) | $d_p$ Calculated ($d_p = 2r_p$) (mm) |
| Tenac | 0.6 | 1.40 (6.9) | 0.2 | 0.80 (5.2) |
| Delrin | 0.5 | 1.32 (6.7) | 0.2 | 0.82 (5.3) |

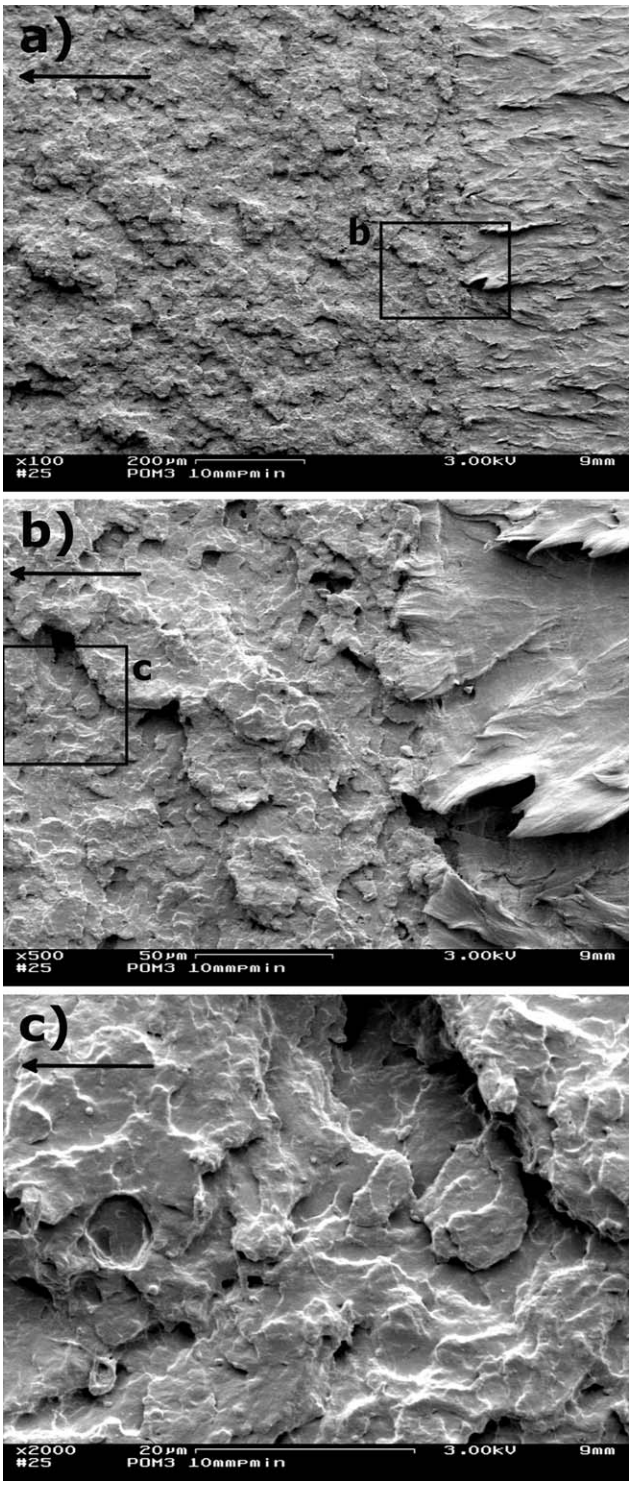


**Figure 5.** Fracture surfaces of monotonically loaded (10 mm $min^{-1}$) Tenac CT specimens analyzed using SEM (arrow indicates crack growth direction).

difference in the surface structure of the spontaneous crack growth area. In the case of Delrin, there are a lot of fine voids in this area (size, ca. 1 µm) which are spread all over the surface [Figure 6(b)]. In contrast, no voids are visible in the case of Tenac [Figure 5(b)]. Even in Figure 5(c), which shows the corresponding surface area with higher magnification, almost no voids are noticeable. This observation was rather unexpected and it suggests that there are differences in the spontaneous crack growth mechanism of the materials. Voiding on fracture surfaces of POM is also reported in the literature (homopolymers[22,24] and copolymers[11]) and in all cases the surface voids were of similar dimension. It has to be emphasized that Bandyopadhyay et al.[22] and Plummer et al.[24] investigated materials with different molecular weights supplied by DuPont (the producer of Delrin). Unfortunately, no literature reference is known which focuses on a detailed fracture analysis of a Tenac resin and thus no confirmation of the lack of surface voids is possible. It was postulated that the voids on the fracture surfaces are a result of the combination of a soft amorphous layer (room temperature is far above the glass transition temperature) and comparatively stiff crystalline lamellae.[11,24] According to both of the studies, a macroscopic load applied on this morphology leads to the formation of the voids and thus causes POM to show similar effects to rubber-toughened polymers. If this was the reason, voiding should also occur in Tenac. However, as mentioned earlier, no literature concerning fracture of Tenac

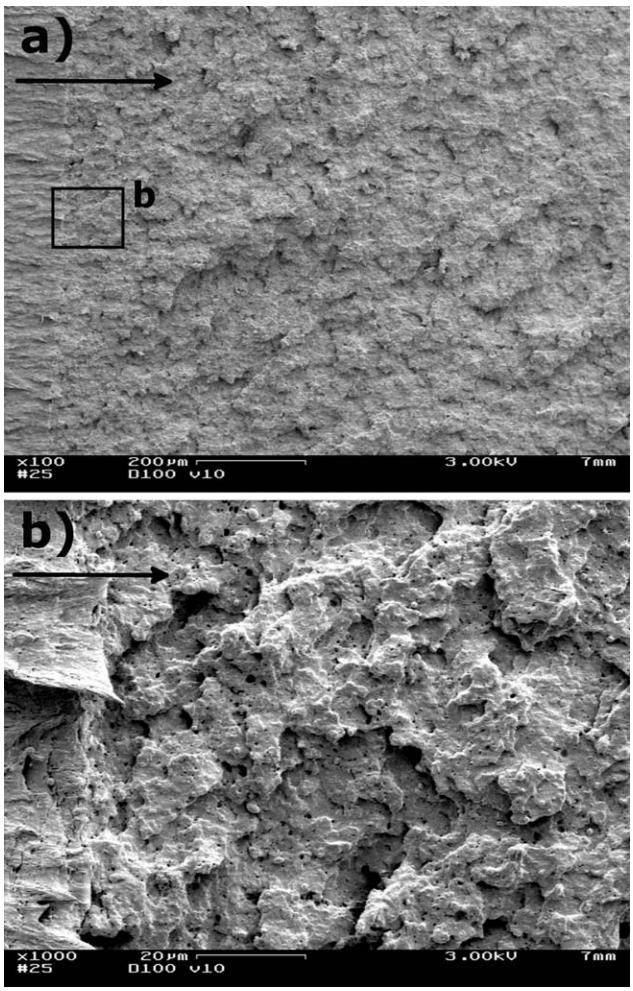


**Figure 6.** Fracture surfaces of monotonically loaded (10 mm $min^{-1}$) Delrin CT specimens analyzed using SEM (arrow indicates crack growth direction).

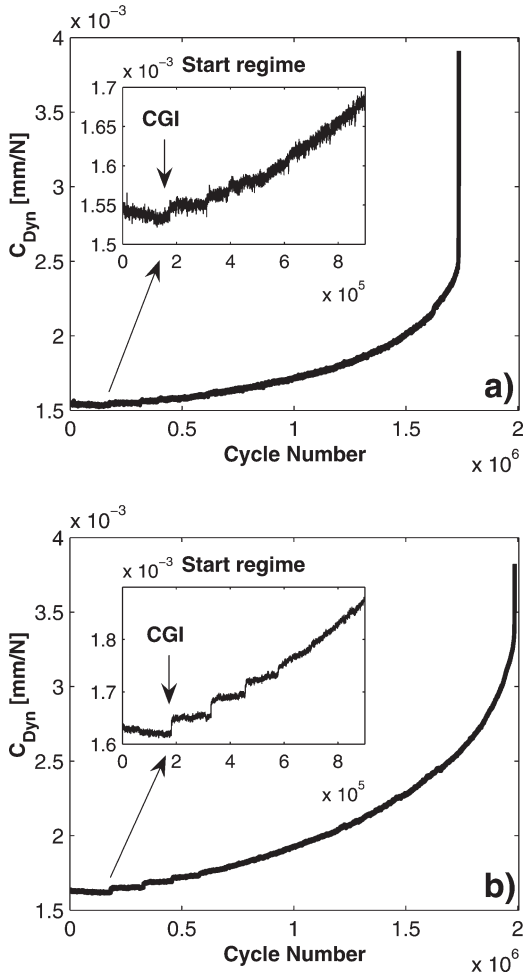


**Figure 7.** Changes in the dynamic specimen compliance during fatigue crack growth tests of POM ($\Delta K_{init} = 2.2$ MPa $m^{0.5}$) with a detailed view of the starting regime and the CGI: (a) Tenac and (b) Delrin.

resins was found and thus the difference in the fracture surface appearance of these very closely related materials is not understood yet. Further research will be necessary to clear up this issue.

**Fatigue Crack Growth Tests.** The mechanical behavior of POM CT specimens during fatigue crack growth tests is shown in Figure 7 (dynamic specimen compliance) and Figure 8 (trend of hysteresis curves). Although the exact trends and shapes of these curves are strongly influenced by $\Delta K$, some general aspects can be deduced.

The dynamic specimen compliance curves shown in Figure 7 reflect the typical behavior for both POM types. Especially interesting is the starting regime which is shown in detail in Figure 7. Generally, $C_{Dyn}$ increases with increasing cycle numbers owing to the length of growing crack. However, after starting the tests (with a razor blade prenotch), $C_{Dyn}$ slightly decreased until a small jump in $C_{Dyn}$ occurred. The small decrease in $C_{Dyn}$ after starting is attributed to the formation of a small craze zone ahead of the crack tip. Owing to the drawing of the fibrils in this zone, the material became stiffer which slightly reduced the compliance of the whole specimen. The following small jump in $C_{Dyn}$ is interpreted as the fracture of the fatigued fibrils in the craze zone and thus it represents the CGI in the specimen. Subsequently, depending on the material and $\Delta K$ level, the formation and breakdown of craze zones was repeated several times or the growth mechanism changed to continuous crack growth. Generally, the discontinuous crack growth (DCG) character was more distinct in the case of Delrin. In the further analysis of the fatigue crack growth tests, the dynamic specimen compliance curves were used for the generation of crack growth kinetics curves.[18]

The hysteresis curve trends shown in Figure 8 provide further information regarding the mechanical behavior of the POM CT specimens during the fatigue crack growth tests. The highest cycle number included in Figure 8 is the last one which was recorded by the testing machine. This means that fracture occurred within the following 1000 cycles and thus the hysteresis curve at this cycle number represents the final mechanical behavior of the specimen. The decreasing slope of the hysteresis curves with increasing cycle numbers reflects the observations in Figure 7 that is the dynamic specimen compliance increases with growing crack lengths. There is a distinct shift of the hysteresis curves along the displacement axis during the tests which is attributed to the combined effect of crack growth and time-

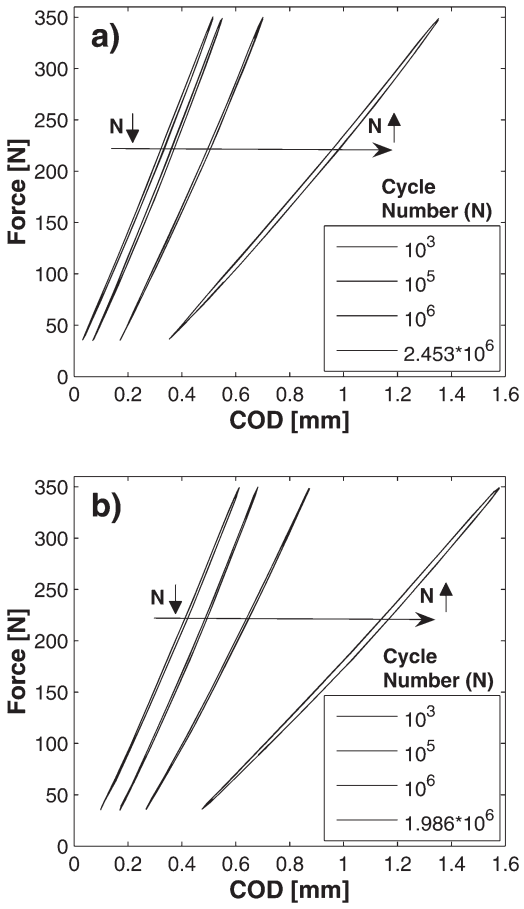


**Figure 8.** Changes in the hysteresis curves (COD, crack-opening displacement) during fatigue crack growth tests of POM ($\Delta K_{init} = 2.2$ MPa $m^{0.5}$): (a) Tenac and (b) Delrin.

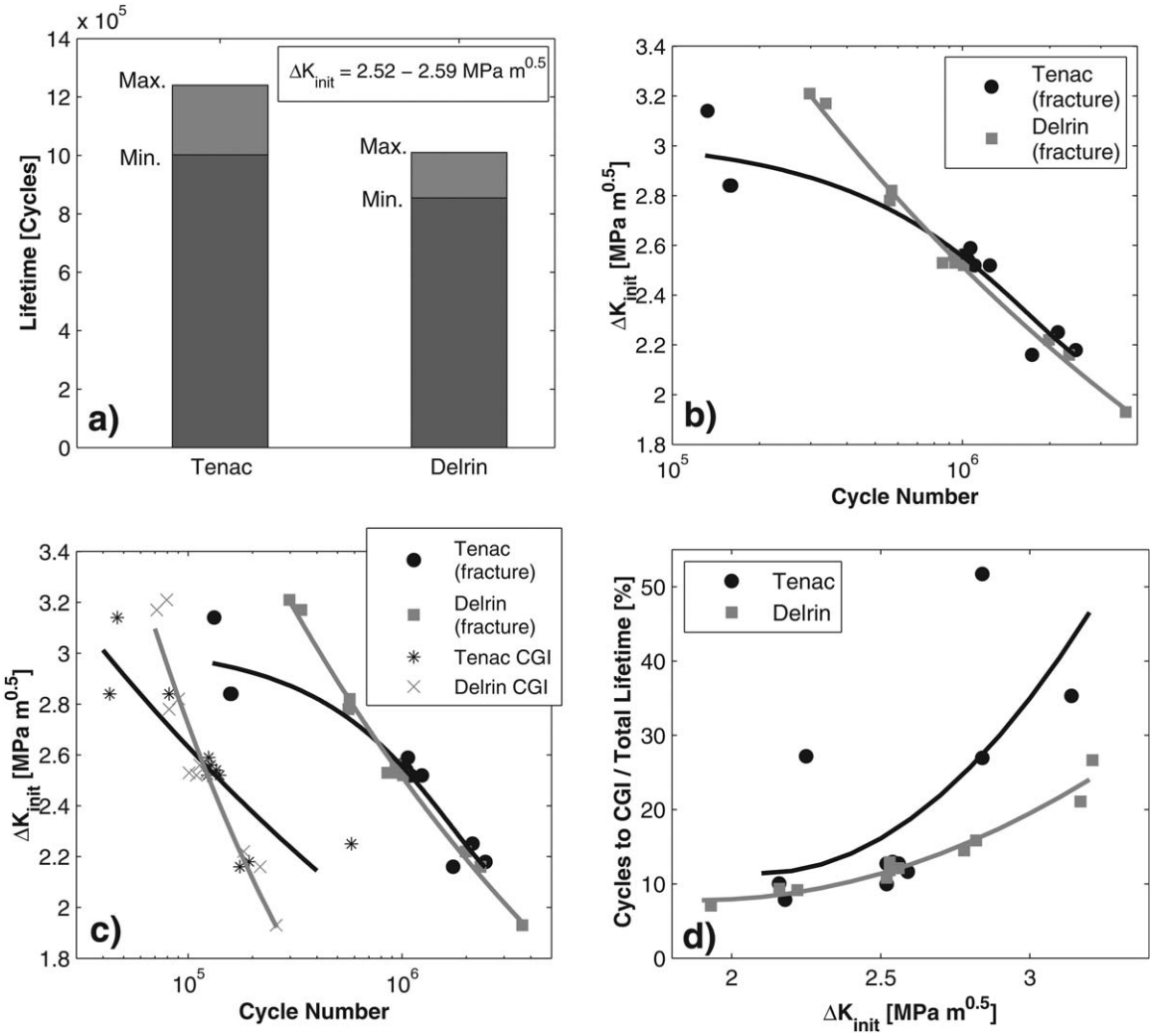


**Figure 9.** Fatigue life-cycle analysis of CT specimens: (a) total life cycles with $\Delta K_{init} = 2.5–2.6$ MPa $m^{0.5}$, (b) total life cycles for various $\Delta(K_{init}$ levels, (c) total life cycles and corresponding cycle numbers to crack growth initiation (CGI), and (d) percentage of CGI on total life cycles.

dependent deformation processes (creep of the material). The qualitative optical evaluation of the irreversible work (area enclosed by the hysteresis curves) shows that this parameter remains approximately constant at the beginning of the fatigue tests. However, at the end of the specimen lifetime it obviously increases. This is correlated with the rising $\Delta K$ level ahead of the crack tip (owing to increasing crack lengths) and the corresponding extension of the plastic zones in the specimen. Observation of selected tests with a thermo camera provided similar results: thermal effects are negligible at the beginning of the test but become more pronounced at the end of the specimen lifetime (last few thousand cycles). Nevertheless, only a very local (ahead of the crack tip) temperature rise with a maximum increase of approximately 10 °C was found. The recorded hysteresis data were also used to perform a quantitative dynamic mechanical analysis of the specimen behavior during the fatigue tests. Unfortunately, neither for the storage and loss parts of specimen compliance and stiffness nor for the loss factor (tan $\delta$), meaningful and uniform results were obtained. These parameters are simply too sensitive to influences introduced by the crack growth process.

In Figure 9, a detailed lifetime analysis of both POM types is shown. It has to be pointed out that the lines drawn in Figure 9(b–d) are added for illustration purposes. Although they represent mathematical trend lines, they were not optimized and especially in the case of the examination of CGI, the scattering is partially very high. The lifecycles of both materials at a defined $\Delta K_{init}$ level of approximately 2.5–2.6 MPa $m^{0.5}$ are compared in Figure 9(a). This level was chosen for this figure as it was the standard testing level with the most convenient test durations. At this $\Delta K_{init}$ level, Tenac shows higher life cycles and a slightly higher scattering in the results than Delrin. According to our experience with other polymeric materials, the scattering in Figure 9(a) is comparatively low and thus a good reproducibility of the experiments at this level can be assumed. In Figure 9(b), a more comprehensive fracture behavior of Tenac and Delrin with varying $\Delta K_{init}$ levels is shown (results shown in Figure 9(a) are contained in this figure). In general, both materials reveal a similar fracture curve at low $\Delta K_{init}$ levels but keeping in mind the logarithmic scale of the $x$-axis and the differences shown in Figure 9(a). At high $\Delta K_{init}$ levels, however, the life cycles of Tenac decrease disproportionally and there is a

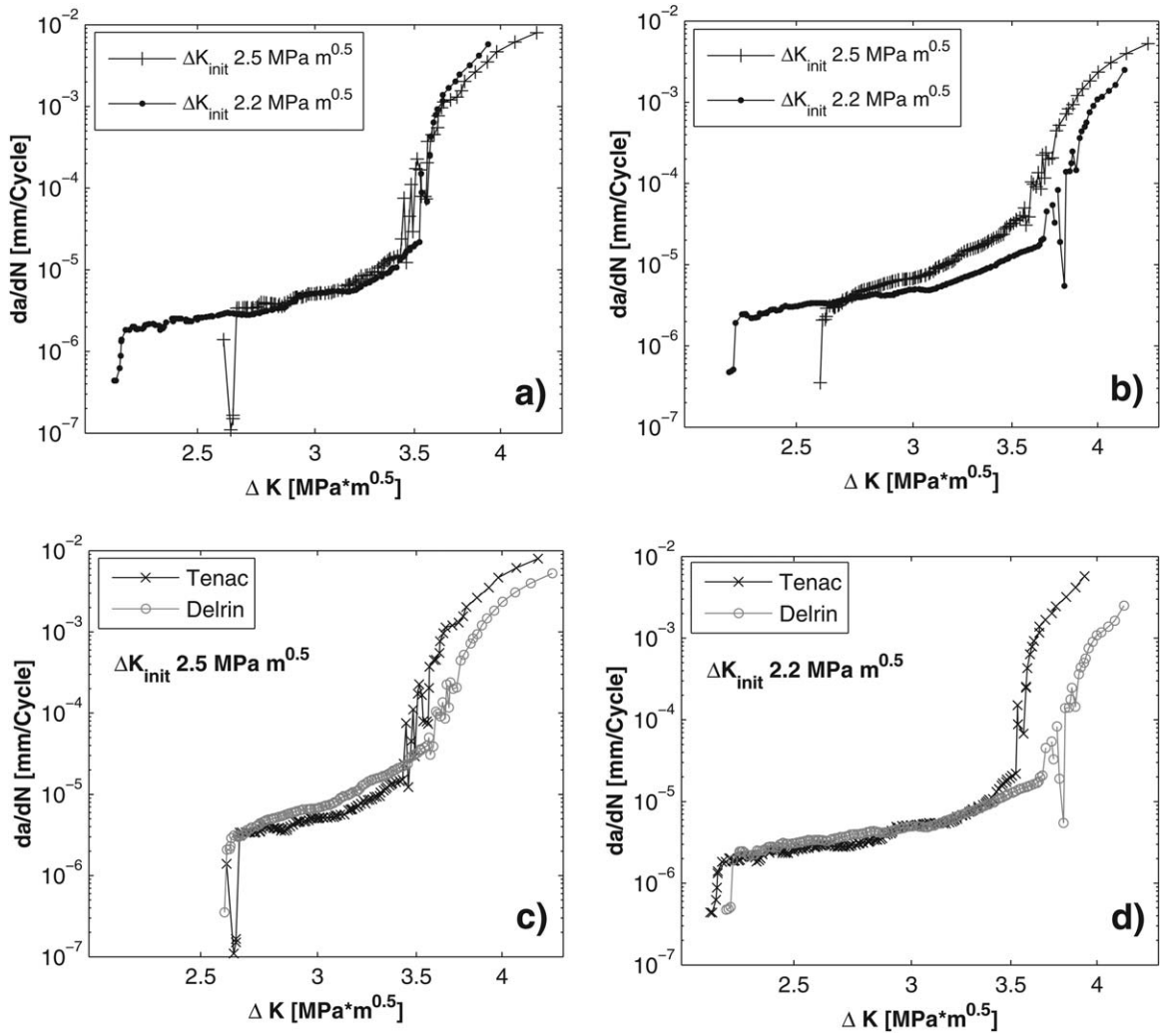


**Figure 10.** Crack growth rates in POM during fatigue crack growth tests: (a) Tenac, (b) Delrin, (c) $\Delta(K_{init} = 2.5$ MPa $m^{0.5}$, and (d) $\Delta(K_{init} = 2.2$ MPa $m^{0.5}$.

strong discrepancy between the materials. The reason for this is expected to be a disproportional increase of the plastic zone ahead of the crack tip owing to the higher $\Delta K_{init}$ levels. Thus, at these levels the applicability of the LEFM concept in conjunction with the rather small specimen widths is already limited. Tenac shows a more distinct scattering in the life cycles than Delrin.

In Figure 9(c), the cycles to CGI are added and compared to the total lifetime of the investigated specimens. In this way, the two main life phases of the samples are differentiated: CGI and crack growth. Similar to the total life cycles, there is almost no scattering in the cycles to CGI in the case of Delrin. In contrast, Tenac reveals a much more intensive scattering. This is also reflected in Figure 9(d) which shows the contribution of the cycles to CGI to the total lifetime. Despite the scattering of the Tenac specimens, it is obvious for both materials that this contribution increases with rising $\Delta K_{init}$ level.

In the following paragraphs, the crack growth regime will be analyzed in more detail. Figure 10 shows crack growth curves of Tenac and Delrin at two different $\Delta K_{init}$ levels. The curves were generated by using the method described by Berer and Pinter.[18] Three classical crack growth regimes are observed in Figure 10. There is the initial crack growth start, the stable crack growth, and the unstable crack growth regime. Generally, the stable crack growth regime of POM was not linear in the double-logarithmic scale. Moreover, slight discrepancies in both shape and slope were even observed between the measurements of the same type (material and $\Delta K_{init}$ level). In Figure 10(a), no significant influence of moderate $\Delta K_{init}$ levels on the crack growth rate ($da/dN$) of Tenac can be noticed. In contrast, Delrin shows a distinct dependence [Figure 10(b)]. Thus, although the crack growth rate of Delrin is higher at $\Delta K_{init} = 2.5$ MPa $m^{0.5}$ (which is approximately the level examined in Figure 9(a)), there is almost no difference in the growth rates of both materials at $\Delta K_{init} = 2.2$ MPa $m^{0.5}$ [Figure 10(c,d)]. Considering the observations made in Figure 9, it is obvious that both materials are differently sensitive to changing $\Delta K_{init}$ levels.

In Figures 11–15, the fracture surfaces of cyclically fatigued POM CT specimens are analyzed. Figure 11 shows the different regimes which can be observed on these surfaces: razor blade

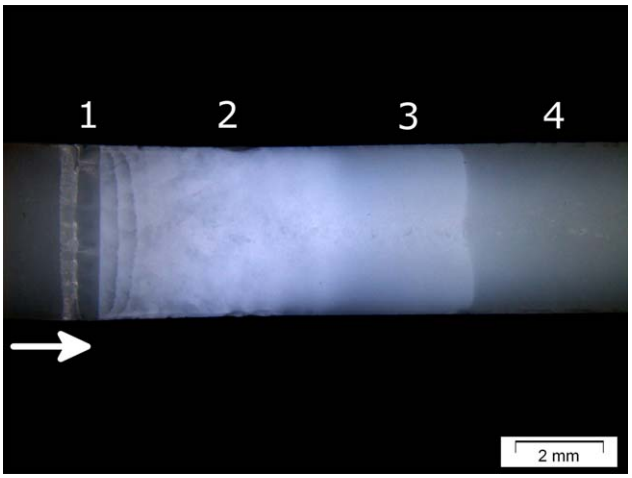


**Figure 11.** Light microscope image of a fracture surface (Delrin) obtained from fatigue crack growth tests of POM CT specimens with a schematic overview of the different surface regimes (arrow indicates crack growth direction): (1) razor blade prenotch, (2) fatigue crack growth regime, (3) transition regime, and (4) spontaneous crack growth. [Color figure can be viewed in the online issue, which is available at wileyonlinelibrary.com.]

prenotch, fatigue crack growth area (stable and unstable crack growth), transition regime, and spontaneous crack growth area. The fatigue crack growth area is characterized by an intense white appearance in the light microscope which was previously observed for POM and other semi-crystalline polymers.[7,23] Owing to the white color, it looks very similar to the plastic zones of the monotonically loaded CT specimens. The intensive white color indicates microvoids within the material which were generated by craze formation during the crack growth process.[15,20,24] After the area of fatigue crack growth, there is a transition regime which is followed by the spontaneous crack growth area. Interestingly, the transition regime is whiter than the area of spontaneous crack growth which does not reveal a significant change in color. It could be speculated that there is a correlation between the transition regime and the unstable crack growth. However, this was proven wrong by measuring the crack lengths at the point of initiation of the transition regime. It was found that the appropriate calculated $\Delta K$ values were almost identical with the last $\Delta K$ values in the corresponding crack growth kinetics curves. Hence, the transition regime was generated between the phases of unstable crack growth and the spontaneous crack growth and it is interpreted as an artifact of the last few life cycles. Regarding the area of spontaneous crack growth, it is supposed that it is closely related to the corresponding zone of monotonically loaded specimens. Similar to the latter one, the crack in this area did not bifurcate but remained within its original growth plane (perpendicular to the direction of loading). However, as the last two regimes do not reflect the fatigue crack growth behavior of the specimens, they were not examined in more detail.

The fatigue crack growth area of both POM types is shown with a higher magnification scale in Figures 12 and 13. Besides the intense white color owing to microvoids, further surface characteristics are visible in both figures. The most obvious ones are the stripes in the starting regime of the Delrin surface in Figure 13. Owing to their dimension and the DCG behavior shown in Figure 7, they are interpreted as DCG bands. This is in accordance with the studies of Bretz et al.[7] and Hertzberg et al.[25] in which various Delrin types were examined regarding their fatigue crack growth properties. It was discussed by Hertzberg et al.[23,26] that for many polymers the width of the DCG band correlates well with the size of the plastic zone according to the Dugdale model (eq. (4)). To test this correlation for Delrin, the width of the first band was estimated and the resulting yield stress was calculated using eq. (4).[23] In the center of the specimen, a (maximum) width of 0.42 mm was obtained which resulted in a calculated (minimum) yield stress of 87 MPa. Considering Figure 2, this value is not realistic and thus it is concluded that for this material the Dugdale model does not describe the size of the plastic zone accurately. The same result was reported for various Delrin types and also for Polyamide 66.[7]

$$d_p = \frac{\Pi}{8}\left(\frac{K_{\max,\mathrm{init}}}{\sigma_y}\right)^2 \quad (4)$$

With $d_p$ being the dimension of the plastic zone; $K_{\max,\mathrm{init}}$ is the initial maximum stress intensity factor ($K_{\max,\mathrm{init}} = \Delta K_{\mathrm{init}}/[1-R]$); $\sigma_y$ is the yield stress; $R$ is the load ratio which was 0.1 in all tests.

The Tenac fracture surface in Figure 12 does not show DCG bands. However, in general, Tenac fracture surfaces showed DCG bands as well but they were less distinctive than those observed for Delrin. This agrees well with the observations made in the compliance curves (Figure 7) in which Delrin generally showed more distinctive discontinuous jumps than Tenac did. Despite the difference in the appearance, the widths of the bands were almost identical for both materials. As the $K_{\max}$ level was identical to that used for the Delrin tests, the yield stress calculated using eq. (4) is also very similar. Thus, the Dugdale model (eq. 4) is not applicable for Tenac either.

It is obvious in Figure 13 that the DCG bands were curved with the maximum width in the center of the specimen and a continuous decrease toward the edges. This and the strong width reduction near the surface are attributed to the changes in the stress state (plane strain to plane stress). Regarding the outermost area, some influence of the specimen surface layer on the DCG band cannot be fully excluded. The intensity of the visual impression of the DCG bands was found to decrease with increasing crack length which is in accordance with the literature.[23] Generally, only the first few bands could be clearly identified although there were also some cases where further DCG band marks were visible in the near surface area of the specimen.

Aside from the white color and DCG bands, the appearance of the fracture surfaces in Figures 12 and 13 looks rather patchy with slight differences between the materials. In both the figures, narrow belts along the near surface areas are observed. In these belts, the materials seem to be deformed more plastically than in the rest of the specimen. As the stress state at this surface area is expected to be predominantly in plane stress, this is not surprising. Nevertheless, it is not fully understood yet if the stress state is the only reason for this effect or if there is also

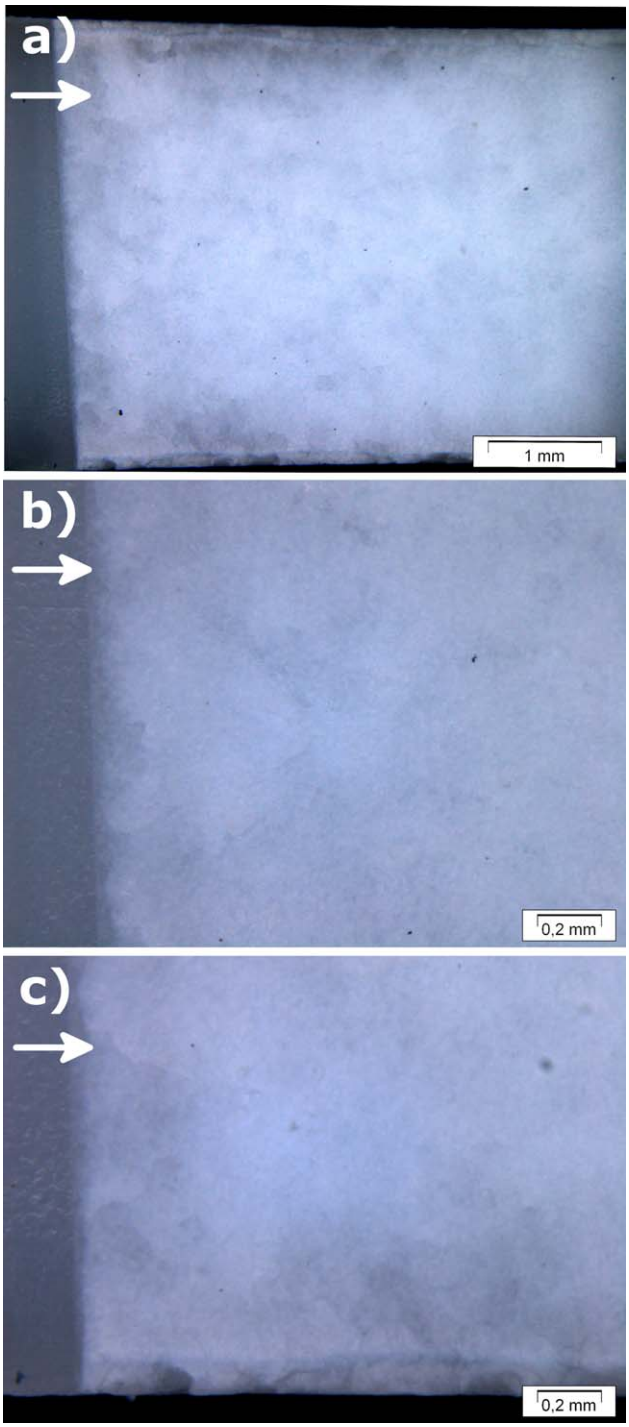


**Figure 12.** Crack growth area on the fracture surface of a cyclically fatigued Tenac CT specimen ($\Delta K_{init} = 2.56$ MPa $m^{0.5}$, arrow indicates crack growth direction): (a) overview, (b) starting regime in the middle of the specimen with higher magnification scale, and (c) starting regime close to the surface with higher magnification scale. [Color figure can be viewed in the online issue, which is available at wileyonlinelibrary.com.]

some influence of the specimen surface layer. At higher $\Delta K$ levels (crack lengths) but still within the fatigue crack growth regime the fracture surfaces were found to become finer except for the middle of the specimen where a rough texture remained.

SEM images of the specimens presented in Figures 12 and 13 are shown in Figures 14 and 15. Surprisingly, the DCG bands, which were clearly visible in the light microscope images, are hardly discernable on the SEM images. They can be identified

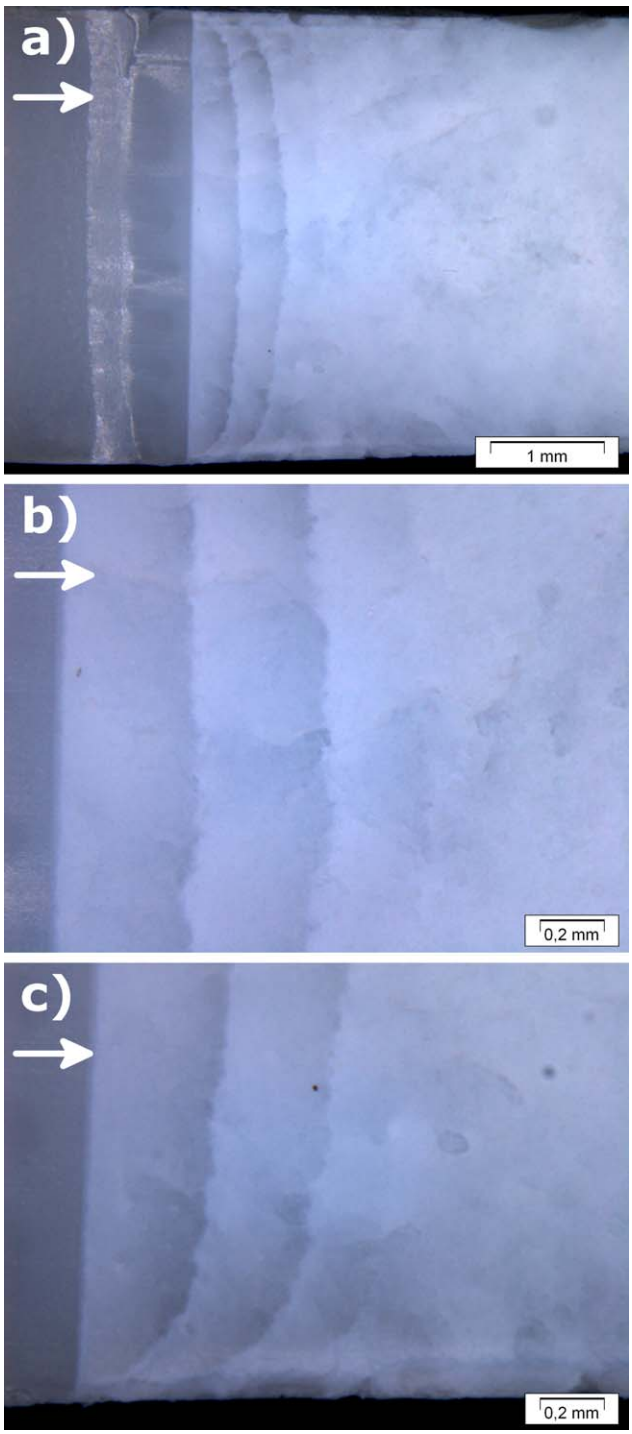


**Figure 13.** Crack growth area on the fracture surface of a cyclically fatigued Delrin CT specimen ($\Delta K_{init} = 2.56$ MPa $m^{0.5}$, arrow indicates crack growth direction): (a) overview, (b) starting regime in the middle of the specimen with higher magnification scale, and (c) starting regime close to the surface with higher magnification scale. [Color figure can be viewed in the online issue, which is available at wileyonlinelibrary.com.]

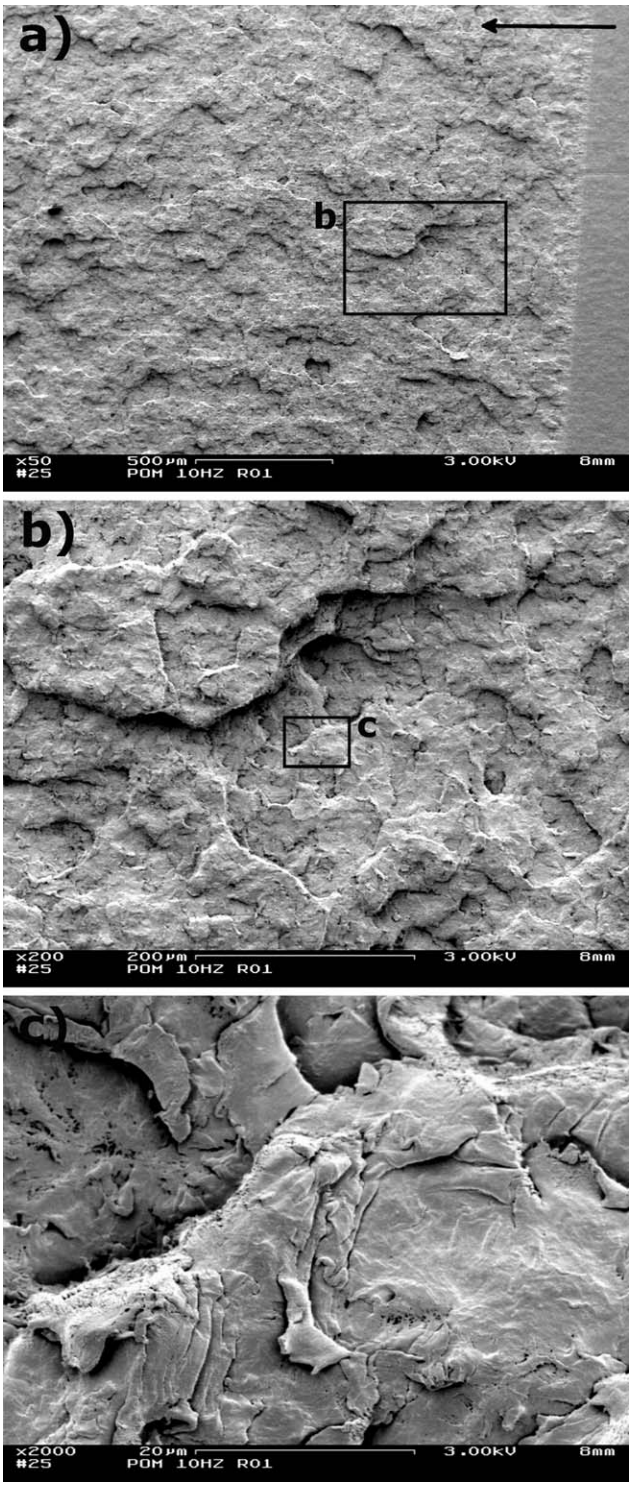


**Figure 14.** SEM images of the Tenac fracture surface shown in Figure 12 (arrow indicates crack growth direction).

only at lower magnification scales in combination with the light microscope images. The surface texture in the fatigue crack growth regime looks very similar to that observed in the spontaneous crack growth regime of the monotonically loaded specimens (Figures 5 and 6). However, in the fatigue crack growth regime, the surface structure is coarser than in the spontaneous crack growth area. Comparing Tenac (Figure 14) and Delrin (Figure 15), some differences are observed. The patches on the surface of Tenac are big in size with a smooth doughy appearance. In some areas, the material seems to be folded and some microvoids (0.5–1 µm) are visible on the surface. In the case of

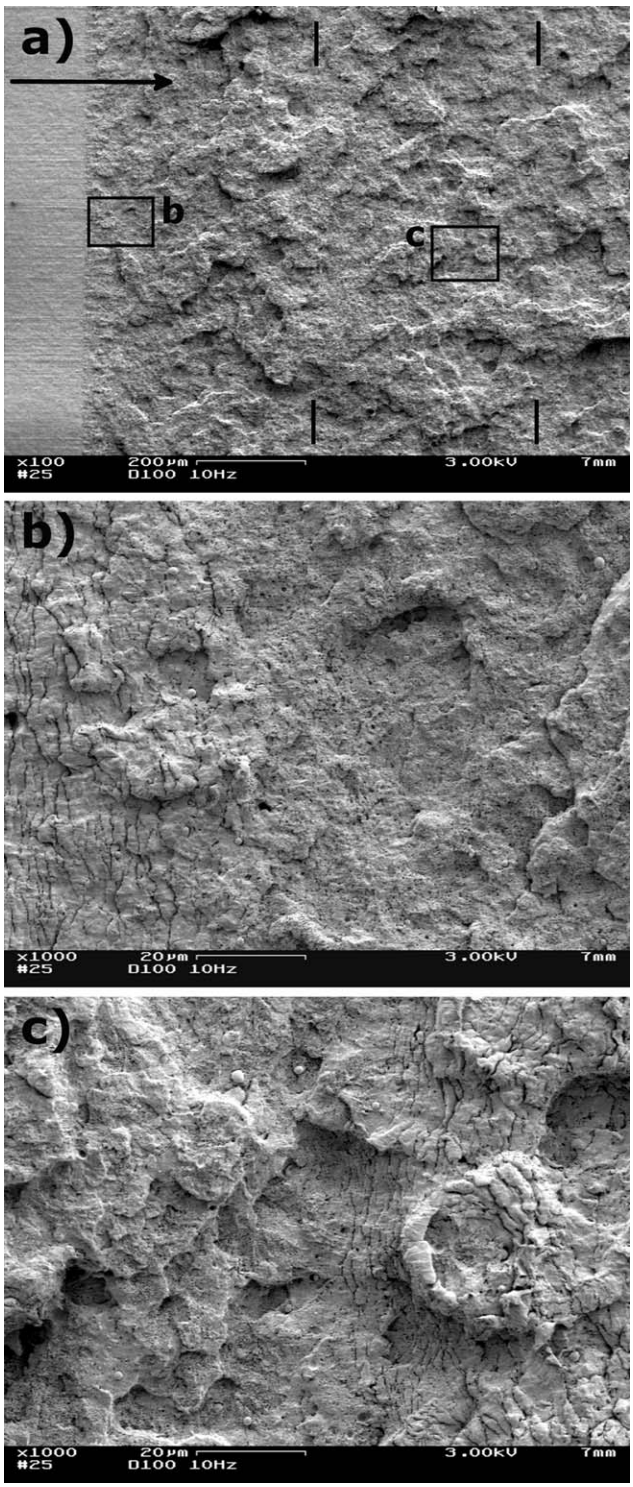


**Figure 15.** SEM images of the Delrin fracture surface shown in Figure 13 (arrow indicates crack growth direction and the lines indicate the position of the DCG bands in Figure 13).

Delrin, the surface has a rough appearance with numerous microvoids (main part: $\leq$1 μm in size) and cracks on the surface. Surface cracks were also partially found for Tenac, but in this case the cracks were accompanied by a doughy and smooth surrounding surface. This is in contrast to the rather rough surrounding surface of Delrin shown in Figure 15. Although there are microvoids on the fatigue crack growth surface of Tenac, there are far fewer in number, which is similar to what was observed for the fracture surfaces of the monotonically loaded specimens. Theoretical considerations for the excessive formation of microvoids in Delrin were already discussed for the monotonically loaded specimens (combination of soft amorphous layer and stiff crystalline lamella). Again, it is unclear at this point about the reason why the formation of microvoids is much less distinctive in the case of Tenac. However, as already mentioned for the monotonically loaded specimens no literature is available regarding this topic. As for the monotonically loaded specimens, no morphological characteristics (e.g., spherullites) are observed on the fracture surfaces of either material which is in accordance with the study by Plummer et al.[24] Nevertheless, spherullitic structures on fatigue crack growth surfaces of different Delrin types are reported in the literature.[7,25]

In this study, the fracture surface region close to the point of CGI was focused on. As the crack growth rates in this regime are very low, it plays a dominant role in the total specimen lifetime. Thus, it was the most appropriate region for a detailed analysis. The regions of unstable and spontaneous crack growth were examined only cursorily. SEM images of Delrin indicated that in the unstable regime the surface is smooth with a lot of parallel surface cracks. In the area of the spontaneous crack growth, a surface texture was observed which was very similar to the corresponding area of the monotonically loaded CT specimens. In the literature, similar surface textures are reported for POM copolymers.[8,11] In both the studies, the parallel surface cracks in the unstable crack growth regime are interpreted as fatigue striations. At the present state of research, this can neither be confirmed nor negated for the materials used in this study. Further examination of these two regions would be necessary to obtain definite results but this would go beyond the scope of this research.

Although the mechanism of crack growth in POM is attributed to the formation and breakdown of craze fibrils,[15,20,24] some questions regarding the surface texture observed in the SEM images remain. Once again, it is emphasized that no structures correlated to morphological characteristics were visible on the fracture surfaces analyzed in this research. Although the microvoids on the fracture surfaces are explained by the combination of soft amorphous layer (room temperature is far above the glass transition temperature) and comparatively stiff crystalline lamellae,[11,24] the origin of the patches and surface cracks is less well understood. An interesting reference concerning the latter is the study by Plummer et al.[24] Therein a thin, notched POM film was loaded in tensile direction and subsequently analyzed in the microscope using polarized light. Ahead of the crack tip a bundle of branched cracks was found. Assuming that there is a similar structure in front of the crack tip of the investigated CT specimens, this can explain both patches and surface cracks. In this case, the patches are explained by the coalescence of cracks growing along different paths and the surface cracks reflect further cracks of the bundle. The discrepancies between fracture surfaces of monotonically and cyclically loaded specimens and between those of Tenac and Delrin are attributed to a varying appearance of this crack bundle. However, it has to be kept in mind that there is a considerable difference in the thickness of the films examined by Plummer et al. (10 μm) and the thickness of the CT specimens investigated in this research (4 mm).[24] Thus, the comparison has to be treated with caution.

Considering the similar molecular weight and weight distribution as well as the identical processing of both materials, we may assume that the observed differences in the morphology are mainly caused by different nucleation. However, it is unclear at this point if the relatively small discrepancies in the morphology are responsible for the deviations observed in the fatigue crack growth tests and also on fracture surfaces. Especially, the spherullite size and distribution was postulated in the literature to have no significant influence on fracture mechanical properties of POM.[8,11,20] This is reasonable because in POM and other polymeric materials the crack path was found to run through the spherullites[7,11,24,25,27–29] as long as the latter do not pass a distinct level of size and crystalline perfection.[24,28] An aspect which has not been considered so far is what was added to the polymer matrix. It is known that there is an influence of additives on the fracture behavior of polymers which was shown for a POM copolymer, for example.[30] As both the materials are commercially available products, no information regarding this issue was available.

Finally, let us discuss some additional aspects which were observed. The fractured CT specimens which were generated during the fatigue crack growth tests were stored in specimen boxes with a closed cover. Every time the box was opened, a pungent smell was noticed which was attributed to formaldehyde owing to chain cutting of the polymer. As the untested specimens did not reveal this smell, it was an accompanying effect of the fatigue tests. Taking into account the study by Plummer et al., this was unexpected because the materials were tested far above the glass transition temperature.[24] In this regime, "disentanglement crazing" rather than "scission crazing" should be the dominant deformation process. Interestingly, Lazzeri et al.[11] found a similar effect for POM copolymers cyclically loaded at high stress levels (with a frequency of 1 Hz). In this case, it was even possible to quantitatively determine the decrease in the molecular weight by using viscosimetric measurements.

## CONCLUSIONS

Two commercially available POM homopolymer resins were investigated regarding their fracture mechanical properties. The results were discussed extensively and compared to the outcome of the previous studies in this field. Although the resins originated from different producers, tensile tests, the analysis of the morphology, and the available information concerning the molecular weight suggested that the two types are closely

related. The fracture mechanical analysis confirmed similarities but there were also slight differences in the results. Some suggestions were made regarding these differences.

Despite the relatively small thickness of the examined CT specimens, it was found that the plastic zones in monotonic fracture tests were smaller than expected for the plane strain condition. For both the materials, the total lifetime of specimens in fatigue crack growth tests could be divided into CGI and fatigue crack propagation. Fatigue crack growth rates were determined and the influence of $\Delta K_{init}$ on the total lifetime was explored. Additionally, the dynamic mechanical behavior of the specimens during the fatigue crack growth tests was analyzed.

No morphological structures were found on the analyzed fracture surfaces. The observed texture was explained on the one hand by the difference in the stiffness of the amorphous layer and crystalline lamellae and on the other hand by a bundle of numerous cracks in front of the crack tip. Both aspects are based on the information found in the literature. Moreover, the appearance of the fracture surfaces confirms that crazing is the mechanism of crack growth in POM. This is in accordance with the literature. Based on a pungent smell of the specimens after the fatigue crack growth tests, it is concluded that scission crazing is at least partially included in the crack growth process.

## ACKNOWLEDGMENTS

The research work of this article was performed at the Polymer Competence Center Leoben GmbH (PCCL, Austria) within the framework of the COMET-programme of the Austrian Ministry of Traffic, Innovation and Technology with contributions by the Montanuniversitaet Leoben (Materials Science and Testing of Plastics). The PCCL is funded by the Austrian Government and the State Governments of Styria and Upper Austria. The authors thank the "Materials Center Leoben Forschung GmbH" and the "Department Materialphysik" at the Montanuniversität Leoben for the possibility of using their X-ray scattering device. In addition, the contribution of Marita Halb and Julia Beter to this research is highly appreciated. Both were involved in the experimental work.

## REFERENCES

1. Saechtling, H.; Oberbach, K. Kunststofftaschenbuch; Hanser: München, **2001**.
2. Domininghaus, H.; Elsner, P.; Eyerer, P.; Hirth, T., Eds. Kunststoffe: Eigenschaften und Anwendungen; Springer: Berlin and New York, **2008**.
3. Heym, B.; Beitz, W. *Konstruktion* **1995**, *47*, 351.
4. Rösler, J. Zur Tragfähigkeitssteigerung thermoplastischer Zahnräder mit Füllstoffen, Dissertation, Germany, **2005**.
5. Berer, M.; Major, Z. *Int. J. Mech. Mater. Des.* **2010**, *6*, 1.
6. Berer, M.; Major, Z. *Strain* **2012**, *48*, 225.
7. Bretz, P. E.; Hertzberg, R. W.; Manson, J. A. *J. Appl. Polym. Sci.* **1982**, *27*, 1707.
8. Runt, J.; Gallagher, K. P. *J. Mater. Sci.* **1991**, *26*, 792.
9. Lesser, A. J. *J. Appl. Polym. Sci.* **1995**, *58*, 869.
10. Lesser, A. *J. Polym. Eng. Sci.* **1996**, *36*, 2366.
11. Lazzeri, A.; Marchetti, A.; Levita, G. *Fatigue Fract. Eng. Mater. Struct.* **1997**, *20*, 1207.
12. Hashemi, S.; Williams, J. G. *J. Mater. Sci.* **1984**, *19*, 3746.
13. Lang, R. W. Applicability of Linear Elastic Fracture Mechanics to Fracture in Polymers and Short-Fiber Composites. Dissertation: Bethlehem, Pennsylvania, USA, **1984**.
14. Lang, R. W.; Balika, W.; Pinter, G. In The Application of Fracture Mechanics to Polymers, Adhesives and Composites; Moore, D. R., Ed.; Elsevier: Amsterdam & Oxford, **2004**; Vol. *33*, p 83.
15. Plummer, C. J. G.; Béguelin, P.; Kausch, H.-H. *Polym. Eng. Sci.* **1995**, *35*, 1300.
16. Baltá-Calleja, F. J.; Vonk, C. G. X-ray Scattering of Synthetic Polymers; Elsevier: Amsterdam & New York, **1989**.
17. Strobl, G. R.; Schneider, M. *J. Polym. Sci. Polym. Phys. Ed.* **1980**, *18*, 1343.
18. Berer, M.; Pinter, G. *Polym. Test.* **2013**, *32*, 870.
19. Ostberg, G. M. K.; Seferis, J. C. *J. Appl. Polym. Sci.* **1987**, *33*, 29.
20. Plummer, C. J. G.; Menu, P.; Cudré-Mauroux, N.; Kausch, H.-H. *J. Appl. Polym. Sci.* **1995**, *55*, 489.
21. Strobl, G. The Physics of Polymers: Concepts for Understanding Their Structures and Behavior; Springer: Berlin and Heidelberg, **2007**.
22. Bandyopadhyay, S.; Roseblade, J. R.; Muscat, R. *J. Mater. Sci.* **1993**, *28*, 3777.
23. Hertzberg, R. W.; Manson, J. A. Fatigue of Engineering Plastics; Academic Press: New York, **1980**.
24. Plummer, C. J. G.; Cudré-Mauroux, N.; Kausch, H.-H. *Polym. Eng. Sci.* **1994**, *34*, 318.
25. Hertzberg, R. W.; Skibo, M. D.; Manson, J. A. *J. Mater. Sci.* **1978**, *13*, 1038.
26. Dugdale, D. *J. Mech. Phys. Solids* **1960**, *8*, 100.
27. Bandyopadhyay, S.; Brown, H. R. *J. Polym. Sci. Polym. Phys. Ed.* **1981**, *19*, 749.
28. Greco, R.; Ragosta, G. *J. Mater. Sci.* **1988**, *23*, 4171.
29. Rae, P.; Brown, E.; Orler, E. *Polymer* **2007**, *48*, 598.
30. Showaib, E. A.; Wyzgoski, M. G. *J. Mater. Sci.* **2002**, *37*, 1895.